WEP Warwick Evans Publishing

International Journal of Natural Resources and Environmental Studies

ISSN: 3006-2012 (Print), ISSN: 3006-0834 (Online) | Volume 8, Number 3, Year 2026
DOI: https://doi.org/10.62051/ijnres.v8n3.04
Journal homepage: https://wepub.org/index.php/IJNRES/index

Experimental Study on Deformation Behavior and Integrity Failure of Cement Sheath in Underground Gas Storage

Yinlong Liang[1, 2, *], Yongjun Hou[1, 2], and Yutian Han[3]

[1]College of Mechanical and Electrical Engineering, Southwest Petroleum University, Chengdu 610500, China;

[2]Oil and Gas Equipment Technology Sharing and Service Platform of Sichuan Province, Southwest Petroleum University, Chengdu 610500, China;

[3]PetroChina Tarim Oilfield Company, Korla 841000, China.

*Corresponding Author: Yinlong Liang

ABSTRACT

The cyclic injection-production operations in underground gas storage (UGS) pose significant challenges to the sealing integrity of wellbore cement sheath under cyclic loading. To elucidate the failure mechanism, this study systematically investigates the deformation behavior and integrity of cement sheath used in UGS through mechanical experiments. Firstly, uniaxial, ambient-temperature triaxial, high-temperature triaxial, and cyclic loading-unloading tests were conducted on set cement to clarify the evolution laws of its mechanical properties. The results indicate that set cement exhibits brittle failure under uniaxial compression. The confining pressure in triaxial tests significantly enhances its strength and ductility, while a high-temperature environment induces a pronounced thermal softening effect, leading to earlier yielding and enhanced plastic deformation. Under cyclic loading, the cement displays a hysteresis loop, with plastic strain accumulating continuously. Furthermore, the upper limit of cyclic stress is identified as the key factor governing its fatigue damage. Based on these findings, engineering application guidance is proposed, focusing on the selection of high-temperature resistant materials and the control of operational pressure. This provides a theoretical basis for ensuring the long-term safe operation of UGS wells.

KEYWORDS

Underground gas storage; Cement sheath; Cyclic pressure; Mechanical properties; Integrity test.

1. INTRODUCTION

With the global adjustment of the energy structure and the surge in demand for natural gas, the scale and operational intensity of Underground Gas Storage (UGS) facilities, which serve as critical infrastructure for regulating supply-demand balance and ensuring energy security, have been increasingly growing. During the long service life of a gas storage well, the wellbore, as the sole channel connecting the subsurface reservoir to the surface, its long-term sealing integrity is paramount for preventing natural gas leakage and ensuring safe operation. The cement sheath, which provides structural support for the casing and isolates formations to achieve zonal isolation, acts as a crucial barrier. Its integrity directly determines the sealing performance of the wellbore. Under the cyclic injection-production conditions typical of UGS operations, the wellbore is subjected to significant alternating internal pressure and temperature loads, subjecting the cement sheath to complex cyclic stress states. This readily induces the initiation and accumulation of damage, such as micro-annuli and shear failure, ultimately leading to barrier failure and posing substantial safety risks.

Therefore, a thorough investigation into the mechanical deformation behavior and failure mechanisms of the cement sheath under cyclic loading holds significant theoretical importance and engineering value. It is essential for establishing scientific evaluation methods for wellbore integrity in UGS, optimizing cementing design and material systems, and enhancing the safe operational capacity of gas storage facilities.

Extensive research has been conducted by scholars concerning the deformation behavior and integrity failure mechanisms of cement sheaths in UGS wells under complex loading conditions, employing methods such as experimental studies, theoretical analysis, and numerical simulation. These investigations aim to provide a theoretical basis for material optimization, structural design, and integrity management.

In terms of experimental research, scholars have systematically investigated the mechanical behavior and failure processes of cement sheaths under complex loading through material testing, full-scale experiments, and microscopic characterization. Regarding the cement material itself, uniaxial/triaxial compression and cyclic loading-unloading tests have revealed the evolution of its strength, toughness, and permeability, as well as the critical influence of temperature[1][3]. Full-scale or simulated wellbore experiments have visually observed interface debonding, microannulus formation, and gas channeling under alternating loads, clarifying that cumulative plastic strain-induced failure at the first interface is the primary cause of sealing failure[4]-[6]. To improve cement sheath adaptability, material modification studies have been widely conducted, incorporating polymers (e.g., EVA), fibers, elastomers, and sustainable materials (e.g., fly ash and eggshell powder) to enhance toughness, reduce modulus, and optimize pore structure[7][10]. In mechanism exploration and testing methods, research has revealed patterns such as cement sheath deformation damage[11] and permeability evolution[12], and innovated direct tensile testing[13] and bonding strength measurement methods[14], providing new means for accurately assessing integrity.

In theoretical and numerical simulation research, studies have advanced along two main directions: analytical models and numerical simulations. In analytical theory, based on the assumption of multi-layer cylinders and elastoplastic theory, models have been established to quantitatively analyze the effects of casing pressure, temperature, pore pressure, and in-situ stress changes on cement sheath stress, displacement, and interface contact state, revealing mechanisms of microannulus generation and changes in the elastic limit internal pressure[15]-[17]. In numerical simulation, by establishing more refined constitutive models (e.g., strain softening, anisotropic damage, fatigue damage models) and using finite element software, the nonlinear response, cumulative plastic strain, and damage evolution of cement sheaths under cyclic loading have been simulated. This systematically evaluates the impact of injection-production pressure, cement mechanical properties, and formation creep (salt rock) on integrity[18]-[19][23]. Additionally, lifespan prediction methods combining theoretical models and experiments[24] and breakthrough pressure evaluation systems[25]have also provided diverse perspectives for integrity assessment.

Although significant progress has been made in existing research, certain limitations remain. Experimental studies have predominantly focused on the performance of cement materials or the behavior of single interfaces under specific loading conditions. Consequently, a systematic revelation of the damage accumulation and evolution laws within the cement stone under the coupled temperature-pressure cyclic loading process characteristic of periodic UGS injection and production is lacking. Theoretical models are often based on idealized geometric and material assumptions, making it difficult to fully capture the complexities of actual downhole conditions, such as non-uniform in-situ stress, initial cementation defects, and the evolution of material nonlinear damage. While numerical simulations have introduced advanced constitutive relationships, systematic investigations and comparative analyses regarding the influence of design parameters on cement sheath integrity remain insufficient. To address these gaps, this study aims to conduct systematic laboratory mechanical experiments to deeply analyze the deformation behavior and failure mechanisms of the cement sheath under cyclic loading.

Through uniaxial compression, triaxial compression, and cyclic loading tests, the mechanical response and deformation characteristics of the cement sheath under various conditions were investigated to thoroughly elucidate its deformation and failure behavior during the injection-production process in gas storage reservoirs. Based on the experimental data, the primary failure mechanisms of the cement sheath were identified. The findings provide guidance for the design, construction, and operation of cement sheaths in gas storage wells.

2. EXPERIMENTAL OVERVIEW

2.1. Test Program Design

The experimental procedure is shown in Fig. 1, and a total of four test schemes were designed as follows:

Uniaxial Compression Test: Ten sets of uniaxial compression tests were conducted on cement specimens numbered 1-1 to 1-10 to simulate the in-situ stress conditions (0 MPa confining pressure) in the upper section of the gas storage wellbore. Based on the plotted stress-strain curves, mechanical parameters such as the initial compressive strength, Poisson's ratio, and elastic modulus of the cement were derived. The study investigated the mechanical behavior and variation trends of cement under uniaxial compression, with further analysis on the influence of different loading rates on its stress response.

Triaxial Compression Test: Twelve sets of conventional triaxial compression tests at room temperature were performed on cement specimens numbered 2-1 to 2-12 to simulate the in-situ stress conditions at various well depths, with confining pressures of 10 MPa, 20 MPa, 30 MPa, and 40 MPa, respectively. The mechanical properties under different confining pressures and loading rates were tested. Stress-strain curves were plotted using the collected data, and key mechanical parameters were calculated and analyzed. By comparing these results with those from the uniaxial tests, the variations in the mechanical properties of cement under different test conditions were thoroughly examined.

High-Temperature Triaxial Compression Test: Under a confining pressure of 20 MPa, two sets of high-temperature triaxial compression tests were conducted on cement specimens 2-13 and 2-14 to study the mechanical response and failure mechanisms of the material in high-temperature environments. Temperatures were set at 60°C and 80°C, respectively, to simulate the temperature conditions at different well depths. By analyzing the plotted stress-strain curves, the influence of different temperatures on the mechanical performance of the cement was assessed. A comparison of the high-temperature results with data from the room-temperature tests revealed the significant impact of temperature on the mechanical properties of the cement sheath.

Triaxial Cyclic Loading-Unloading Test: Five sets of triaxial cyclic loading-unloading tests were conducted on cement samples numbered 5-1 to 5-5. Five different stress levels were applied: 7-14 MPa, 11-18 MPa, 15-22 MPa, 5-28 MPa, and 10-33 MPa. Based on the plotted stress-strain curves, the variation patterns of the stress-strain relationship under different stress levels were analyzed. A detailed discussion was provided on the failure characteristics of the cement under cyclic loading conditions.

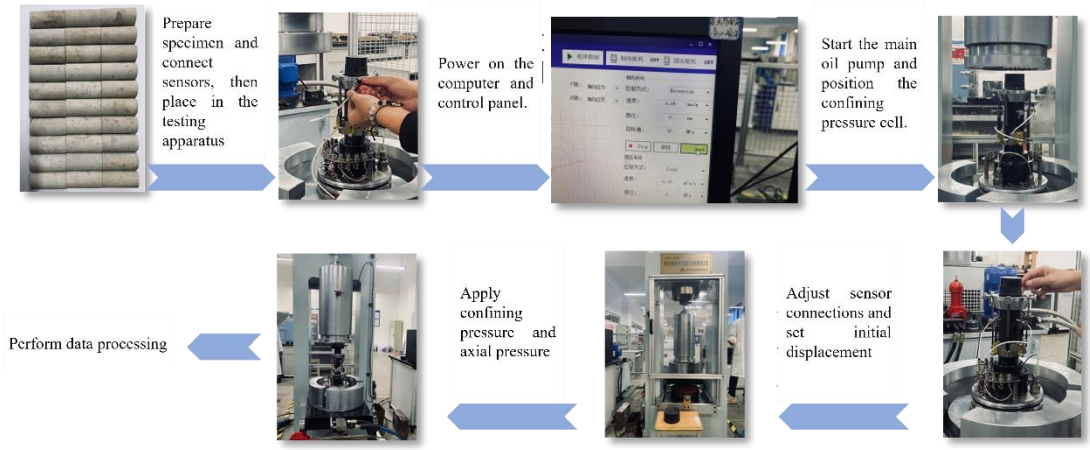

Fig. 1 Experimental flowchart

2.2. Preparation of Test Rock Specimens

The cement formulation used in this study was derived from the conventional-density, flexible cement slurry employed in the well cementing operation of underground gas storage well PG2-QKP1. The cement slurry formulation consisted of: 550 g of cement + 250.25 g of additives + 6.6 g of latex modifier + 44 g of latex + 16.5 g of fluid loss additive + 4.4 g of retarder + 269.5 g of water.

In accordance with the experimental requirements, the cement specimens were fabricated following international standards to ensure their dimensions conformed to the equipment specifications. The specimens were cylindrical with a diameter of 25 mm and a height of 50 mm, as illustrated in Fig. 2a. To guarantee dimensional consistency (with a tolerance not exceeding 0.1 mm), samples with rough surfaces or cracks were discarded. This process aimed to enhance the reliability and accuracy of the test results and to provide high-quality specimens for the study of the mechanical properties of cement in gas storage applications. The prepared test samples are presented in Fig. 2b.

(a) (b)

Fig. 2 Cement specimens. (a) specimen dimensions. (b) actual specimens.

2.3. Testing Equipment

The uniaxial compression, conventional triaxial compression, and cyclic loading tests were all conducted using the computer-controlled electro-hydraulic servo rock testing system depicted in Fig. 3. Users can set the loading mode, rate, and limits via a computer interface to achieve automated loading. The system supports tests such as uniaxial, triaxial, and tensile tests, and is capable of real-time data acquisition and processing. It accurately determines rock properties including compression, tension, and shear characteristics, providing reliable support for engineering evaluation and scientific research.

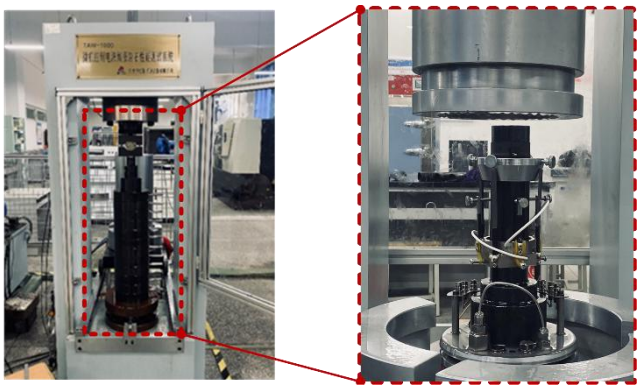

Fig. 3 Computer-controlled electro-hydraulic servo rock testing system

The high-temperature triaxial compression tests were performed using the high-temperature and high-pressure integrated rock testing system illustrated in Fig. 4. Prior to the start of the experiments, the RTR-1500 computer was used to preset and control the test conditions for each specimen. During the testing process, data were collected in real time by sensors attached to the specimens. The computer simultaneously monitored and analyzed the variations in the stress-strain curves of the cement to ensure the accuracy and reliability of the experimental data.

Fig. 4 High-temperature and high-pressure integrated rock testing system

3. ANALYSIS OF CEMENT DEFORMATION CHARACTERISTICS

3.1. Uniaxial Compression Tests

3.1.1. Test Method

Standard cement specimens, fabricated using the cement slurry formulation from gas storage well cementing operations, were subjected to room-temperature uniaxial mechanical tests. Specimens numbered 1-1 to 1-10 were tested in pairs at loading rates of 0.03, 0.04, 0.05, 0.06, and 0.1 mm/min, respectively. Axial strain, radial strain, and axial force were recorded during the tests.

3.1.2. Analysis of Test Results

After testing, the strain-compressive strength curves of the specimens were plotted, as presented in Fig. 5, and the post-test conditions of the specimens are shown in Fig. 6. During the conventional uniaxial compression tests, the deformation and failure process of the specimens could be divided into four stages: (1) Both radial and axial strains exhibited an inclined straight line, indicating elastoplastic deformation due to the gradual compaction of pores and cracks. (2) The stress-strain curve displayed a linear relationship, representing the elastic stage. (3) The stress-strain curve became convex upward, where significant propagation of microcracks under axial load led to structural failure. (4) Macroscopic fracture slip occurred, accompanied by a sharp decline in compressive capacity.

Results from numerous uniaxial compression tests indicate that, although different loading rates exert certain influences on the compressive strength, elastic modulus, and Poisson's ratio of the cement, the deformation characteristics consistently follow similar patterns. The statistical results are summarized in Table 1.

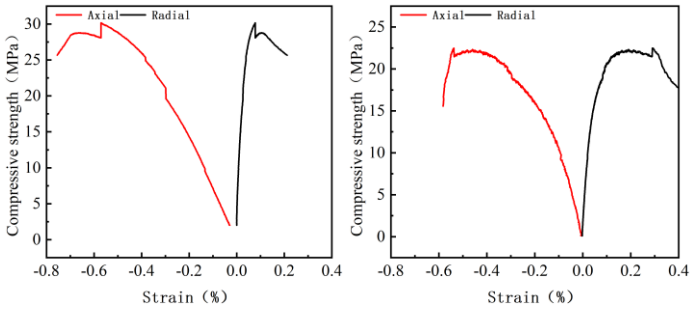

(a) 1-1

(b) 1-2

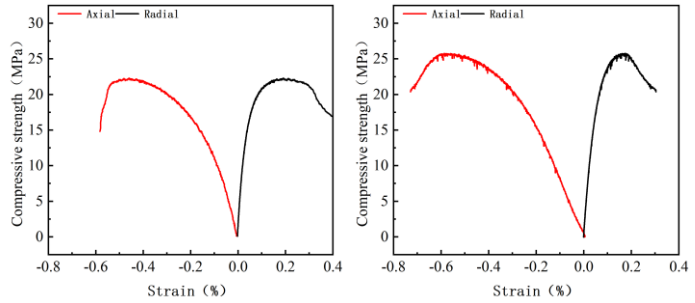

(c) 1-3

(d) 1-4

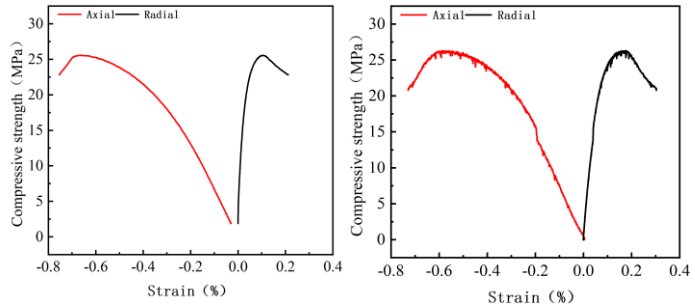

(e) 1-5

(f) 1-6

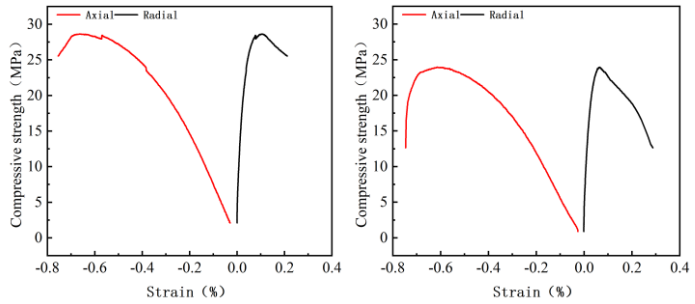

(g) 1-7

(h) 1-8

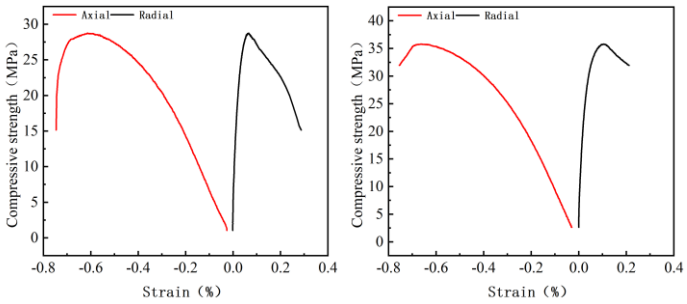

(i) 1-9 (k) 1-10

Fig. 5 Stress-strain curves of cement in uniaxial compression tests

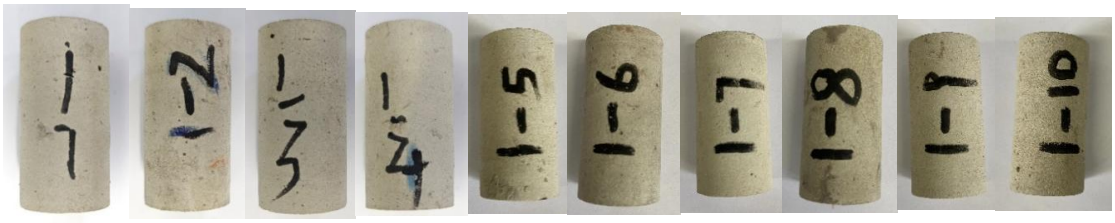

Fig. 6 Morphology of cement specimens after uniaxial compression tests

Table 1 Statistical results of uniaxial compression tests

Numble	Compressive Strength(MPa)	Elastic Modulus(GPa)	Poisson's Ratio	Loading Rate(mm/min)
1-1	23.52	4.99	0.06	0.03
1-2	21.99	5.23	0.08	0.03
1-3	21.76	10.77	0.19	0.04
1-4	25.63	7.88	0.19	0.04
1-5	24.91	4.41	0.04	0.05
1-6	26.84	3.54	0.05	0.05
1-7	27.43	6.35	0.12	0.06
1-8	27.56	6.78	0.15	0.06
1-9	34.32	9.04	0.21	0.1
1-10	35.12	8.44	0.19	0.1

Fig. 7 shows the variation curves of compressive strength, elastic modulus, and Poisson's ratio under different loading rates. The average compressive strengths of the specimens at loading rates of 0.03 mm/min, 0.04 mm/min, 0.05 mm/min, 0.06 mm/min, and 0.1 mm/min were 22.76 MPa, 23.70 MPa, 25.27 MPa, 27.51 MPa, and 34.72 MPa, respectively. As the loading rate increased, the compressive strength also gradually increased, while no clear trend was observed for the elastic modulus or Poisson's ratio. This is because increasing the loading rate induces compressive stress within the cement, and this stress intensifies with higher loading rates. Under compressive stress, the pores and microcracks inside the cement are further compressed, leading to an upward trend in compressive strength. The behavior before the peak stress is nearly linear-elastic. After the specimen's stress reaches its peak strength, the rate of strength decline becomes faster, indicating that higher loading rates make the specimen more prone to failure after reaching its maximum strength.

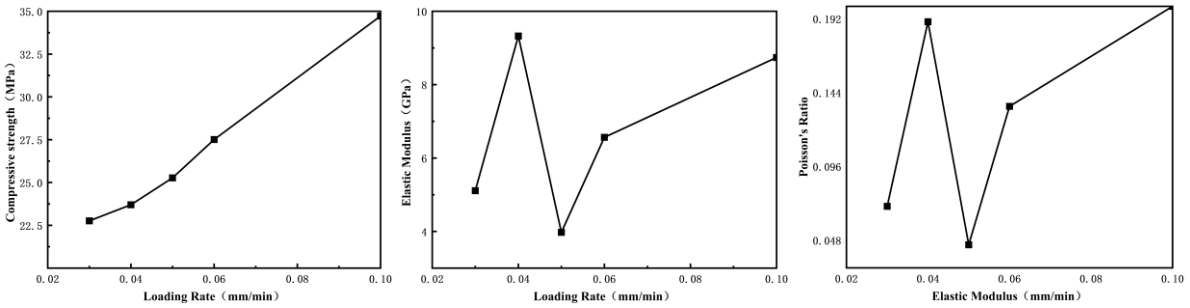

(a) (b) (c)

Fig. 7 Mechanical properties of cement versus loading rate

3.2. Conventional Triaxial Compression Tests

3.2.1. Test Method

In this series of conventional triaxial compression tests, the mechanical properties and deformation behavior of cement under various combinations of loading rates and confining pressures were investigated. The specific test conditions are summarized in Table 2:

Table 2 Conventional triaxial compression test conditions

Numble	Loading Rate(mm/min)	Confining Pressure(MPa)	Notes
2-1	0.03	10	
2-2	0.05	10	
2-3	0.07	10	
2-4	0.03	30	
2-5	0.05	30	
2-6	0.07	30	
2-7	0.03	20	
2-8	0.05	20	
2-9	0.07	20	
2-10	0.1	20	
2-11	0.1	20	Poor sealing performance
2-12	0.1	40	

3.2.2. Analysis of Test Results

By statistically processing the strain and compressive strength data collected during the loading process, the strain-compressive strength curve of the specimen is presented in Fig. 8. This curve illustrates the entire process from the elastic stage to yielding and ultimately to failure, revealing the deformation characteristics of the material under different stress levels. Furthermore, the appearance and failure morphology of the specimens were documented after testing. Details such as crack distribution and fracture surface characteristics are clearly shown in Fig. 9, providing a visual basis for further analysis of the specimen failure mechanism.

The results indicate that under triaxial compression conditions, the compressive performance, stiffness, and Poisson's ratio of the cement all significantly improved. Its load-bearing capacity and deformation resistance were superior to those observed in the uniaxial tests. When approaching the peak compressive strength, the strain exhibited a steep decline, reflecting the elastoplastic characteristics of the material. Specimen 2-11, which had relatively poor sealing performance, showed lower compressive strength but higher elastic modulus and Poisson's ratio, highlighting the important influence of sealing integrity on the mechanical properties of the cement. Meanwhile, the triaxial failure mode primarily manifested as multiple shear cracks, and the deformation process could

also be divided into four stages. The statistical results of the experimental data are presented in Table 3

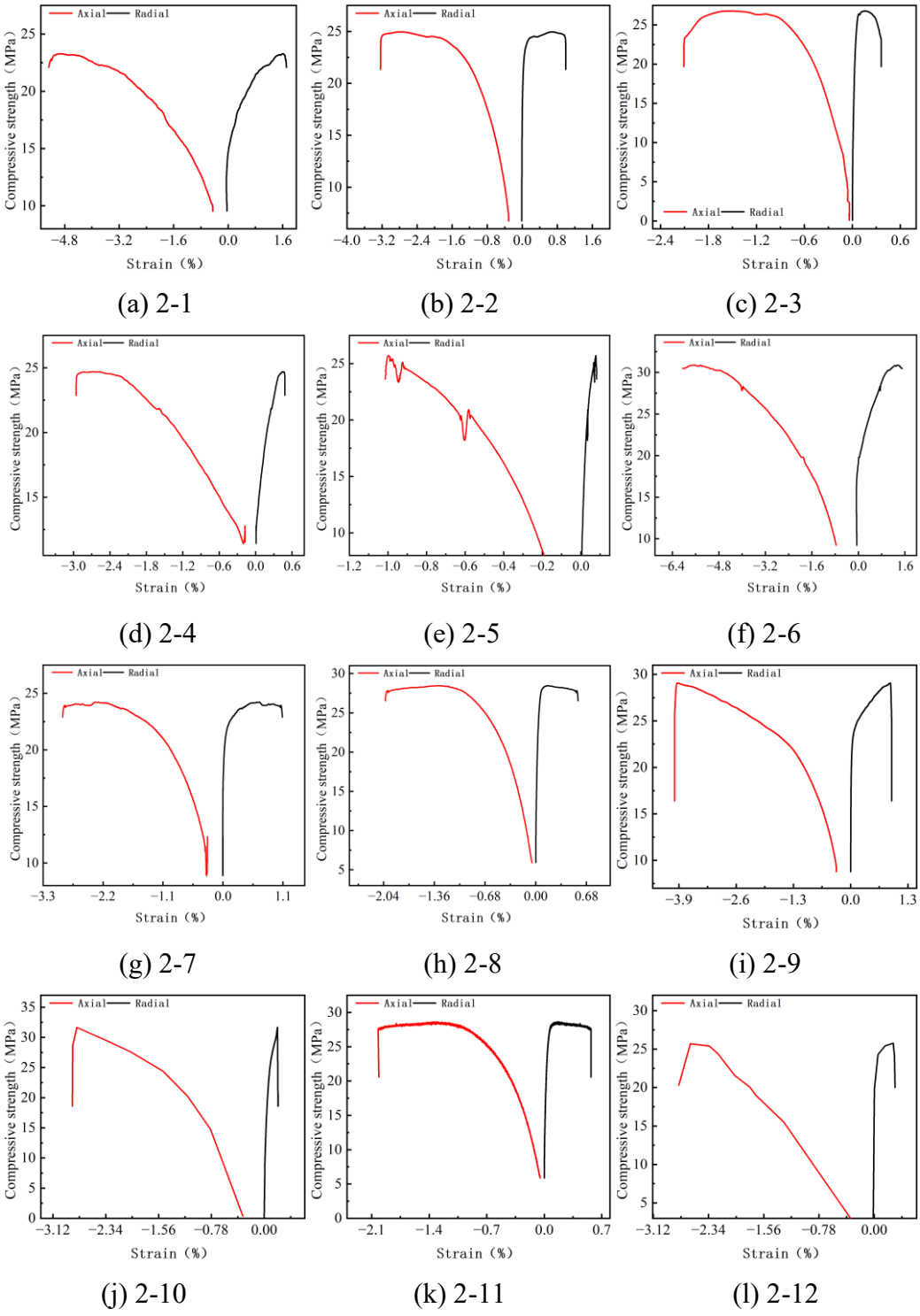

Fig. 8 Stress-strain curves of cement in conventional triaxial compression tests

Fig. 9 Morphology of cement specimens after conventional triaxial compression tests

Table 3 Statistical results of conventional triaxial compression tests

Numble	Compressive Strength(MPa)	Elastic Modulus(GPa)	Poisson's Ratio	Loading Rate(mm/min)	Confining Pressure(MPa)
2-1	22.74	2.49	0.05	0.03	10
2-2	24.77	3.59	0.05	0.05	10
2-3	26.44	3.45	0.06	0.07	10
2-4	24.39	0.32	0.27	0.03	30
2-5	27.16	0.44	0.02	0.05	30
2-6	29.99	0.53	0.06	0.07	30
2-7	23.90	1.01	0.01	0.03	20
2-8	27.92	1.28	0.01	0.05	20
2-9	28.26	1.38	0.01	0.07	20
2-10	52.14	6.39	0.073	0.1	20
2-11	43.94	6.96	0.11	0.1	20
2-12	46.04	3.28	0.027	0.1	40

As shown in Fig. 10, under the same confining pressure conditions, analysis of the influence of different principal stress loading rates reveals that an increase in the loading rate significantly enhances the compressive strength of the specimens. The primary reason for this phenomenon is that at lower loading rates, cracks within the specimen have sufficient time to propagate and generate plastic deformation, leading to failure at relatively low strength. In contrast, at higher loading rates, the rates of crack development and plastic deformation cannot keep pace with the rapid stress increase. Consequently, the cracks are continuously compacted, thereby improving the overall material strength and causing failure to occur only at higher stress levels.

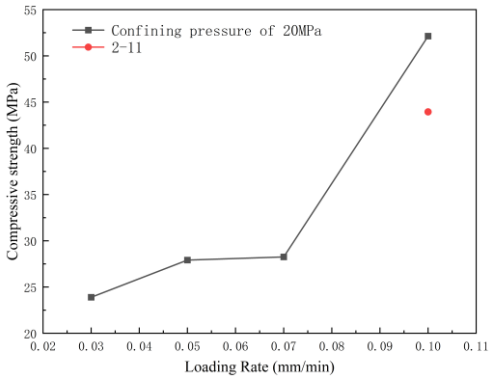

Fig. 10 Compressive strength versus loading rate under 20 MPa confining pressure

As illustrated in Fig. 11, with the principal stress loading rate fixed at 0.03 mm/min, the compressive strength of the specimens shows an increasing trend as the confining pressure rises, while the elastic modulus gradually decreases. The primary reason for this phenomenon is that the confining pressure provides a circumferential confinement effect, significantly inhibiting the propagation of cracks along the circumferential direction within the specimen, thereby enhancing its overall compressive capacity. Concurrently, the presence of confining pressure reduces the elastic modulus of the cement specimens, though this reduction effect diminishes as the confining pressure increases further.

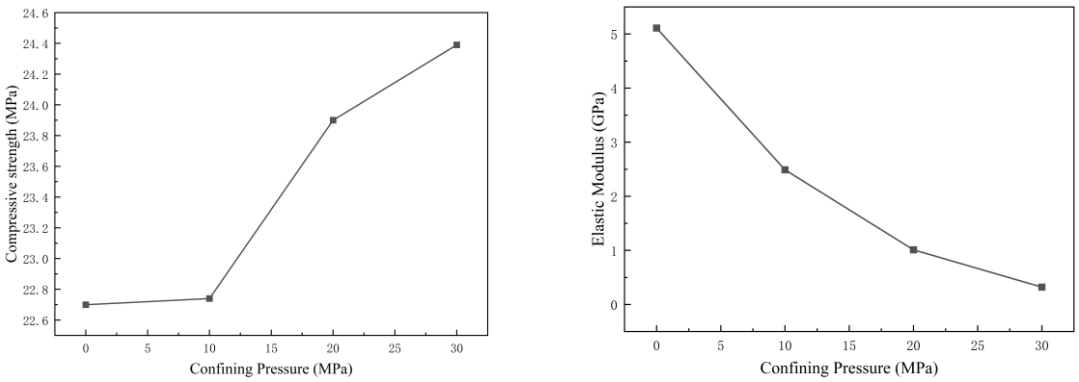

Fig. 11 Compressive strength and elastic modulus versus confining pressure at a loading rate of 0.03 mm/min

In summary, both the principal stress loading rate and the confining pressure significantly influence the load-bearing capacity of the cement specimens. The higher these two factors are, the greater the compressive strength of the specimens becomes. Additionally, an increase in confining pressure leads to a notable rise in both initial and cumulative plastic strain.

3.3. High-Temperature Triaxial Compression Tests

3.3.1. Test Method

Considering that the cement sheath, after setting, fully contacts the formation and its temperature approximates reservoir conditions, high-temperature triaxial compression tests on cement must be conducted to accurately reflect the actual mechanical performance of the downhole cement sheath. The test conditions are summarized in Table 4:

Table 4 Conditions for high-temperature triaxial tests

Numble	Loading Rate (mm/min)	Confining Pressure (MPa)	Temperature (℃)
2-10	0.1	20	25
2-13	0.1	20	60
2-14	0.1	20	80

3.3.2. Analysis of Test Results

Based on the actual operating conditions of the gas storage wellbore, high-temperature triaxial tests at 60°C and 80°C were conducted to evaluate the mechanical performance of the cement. The results, as illustrated in Fig. 12, show that the stress-strain curve of the cement at 60°C still exhibits a favorable elastoplastic trend, indicating that the microstructure remains largely intact under initial thermal stress. However, at 80°C, the compressive strength significantly decreases, and the stress-strain curve yields earlier, fully reflecting the pronounced weakening effect of high temperature on its mechanical properties. This suggests that the internal cohesive strength and skeletal structure of the material are compromised under high-temperature conditions, shifting its mechanical response from predominantly elastic to predominantly plastic deformation. This phenomenon not only reflects the inherent thermal softening effect of the cement at elevated temperatures but also highlights the necessity of thoroughly considering the impact of temperature on cement sheath performance in engineering applications, with appropriate measures taken to ensure operational safety.

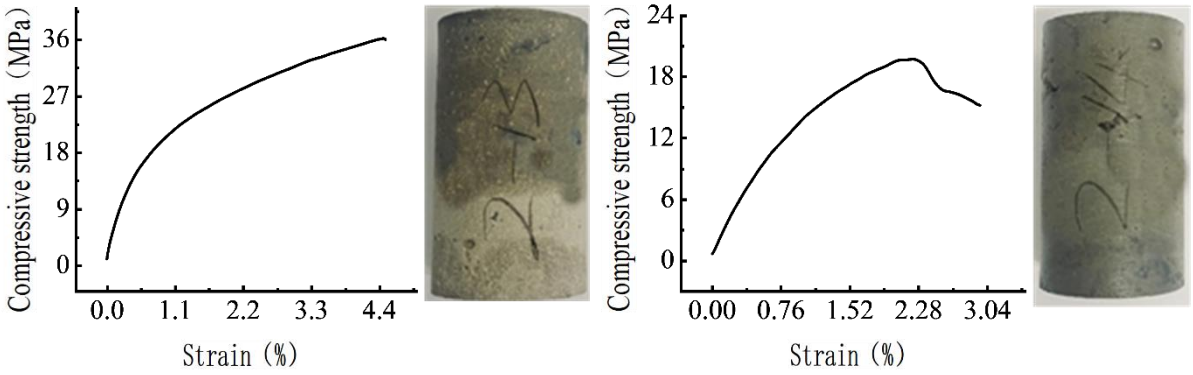

Fig. 12 Stress-strain curves of the cement sheath at different temperatures

The experimental results are presented in Table 5. At temperatures of 60°C and 80°C, both the compressive strength and elastic modulus of the set cement exhibited significant degradation. In contrast, at ambient temperature, the set cement maintained a relatively high compressive strength and a linear-elastic response, indicating that its microstructure remained relatively stable under room-temperature conditions. These changes suggest that high-temperature conditions not only weaken the load-bearing capacity of the set cement but also induce microstructural rearrangement within the material, thereby affecting its overall mechanical properties.

Table 5 Statistical results of high-temperature triaxial compression tests

Numble	Compressive Strength(MPa)	Elastic Modulus(GPa)	Poisson's Ratio	Loading Rate(mm/min)	Confining Pressure(MPa)	Temperature(℃)
2-10	52.14	6.39	0.073	0.1	20	25
2-13	36.3	1.628	0.04	0.1	20	60
2-14	20	1.346	0.02	0.1	20	80

3.4. Cyclic Loading Tests

3.4.1. Test Method

The waveform curve for applying cyclic loads to the cement sheath is shown in Fig. 13, where and represent the upper and lower pressure limits of gas storage operation, respectively. The stress level in the cement sheath under operational pressure is approximately 70% of its compressive strength. Therefore, 70% of the cement sheath's compressive strength was selected as the upper cyclic stress limit to simulate the stress fluctuations experienced during injection and production pressure changes. Based on this, four sets of cyclic stress levels were established, with their upper stress limit being 0.7 times the operational upper pressure limit. To investigate the fatigue characteristics of cement under high-stress conditions, a fifth load set was defined, with its upper stress limit being 0.825 times the operational upper pressure limit. The lower stress limit for each load set was set at 0.4 times the operational lower pressure limit. During the test, the following loading and unloading path was followed:

(1) The axial stress was gradually increased from zero to the upper stress limit σ_{max} at the set loading rate, then unloaded to the lower stress limit σ_{min}, completing the first loading-unloading cycle.

(2) Subsequently, the stress was loaded from σ_{min} to σ_{max} and then unloaded to σ_{min}, completing the second cycle.

(3) The above steps were repeated continuously. Considering that a gas storage well typically undergoes one cycle per year, 15 cycles were performed for each test group to simulate 15 years of injection-production operation.

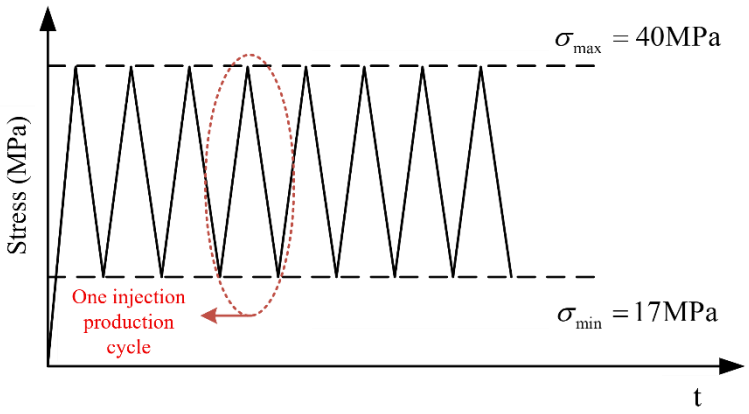

Fig. 13 Loading and Unloading Waveform Curve

Specific cyclic stress levels applied in the tests were: 7~14 MPa, 11~18 MPa, 15~22 MPa, 5~28 MPa, and 10~33 MPa. The test conditions for different specimens are detailed in Table 6, with loading and unloading rates set at 0.1 mm/min and a confining pressure of 20 MPa.

Table 6 Cyclic loading test conditions

Numble	Cyclic Pressure Limits (MPa)	Loading Rate(mm/min)	Unloading Rate(mm/min)	Confining Pressure (MPa)	Cycle Number
5-1	7~14	0.1	0.1	20	15
5-2	11~18	0.1	0.1	20	15
5-3	15~22	0.1	0.1	20	15
5-4	5~28	0.1	0.1	20	15
5-5	10~33	0.1	0.1	20	15

3.4.2. Analysis of Test Results

Fig. 14 illustrates the stress-strain relationship of the cement under different cyclic loadings. The application of cyclic loads results in the formation of distinct hysteresis loops in the stress-strain curves. With an increasing number of cycles, these hysteresis loops progressively shift to the right, indicating the continuous accumulation of plastic strain. Taking Fig. 14a as an example, during repeated loading and unloading within the 7~14 MPa range, the first cycle induced the largest plastic strain, and the incremental plastic strain from each subsequent cycle gradually decreased. Fig. 15 shows that although no obvious macroscopic failure occurred in the specimen, fine microcracks appeared on its surface. Subsequent axial loading led to failure at a compressive strength of 29.84 MPa. Figs. 14b, c, d, and e exhibit a similar trend of cumulative deformation, fully reflecting the typical elastoplastic deformation characteristics of cement under cyclic loading. The statistical results of the experimental data are presented in Table 7.

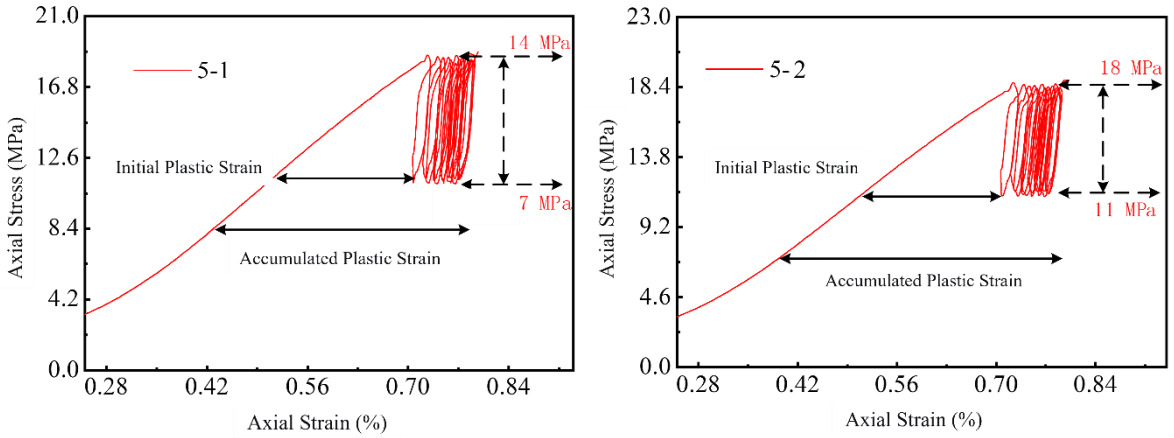

(a) 5-1

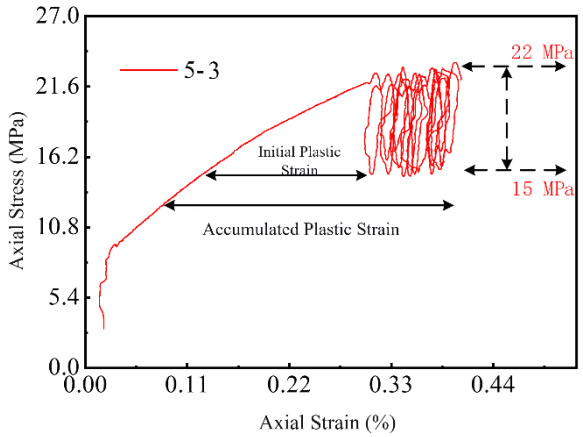

(b) 5-2

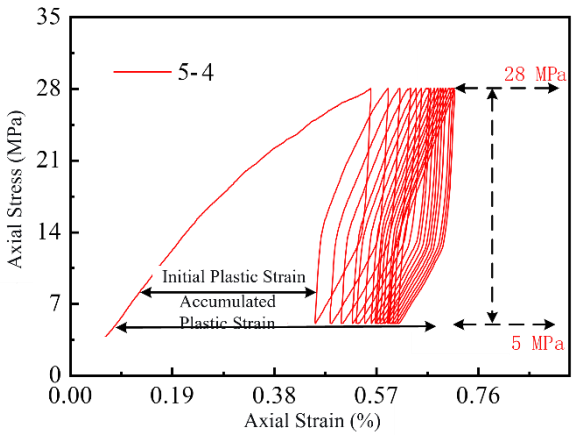

(c) 5-3

(d) 5-4

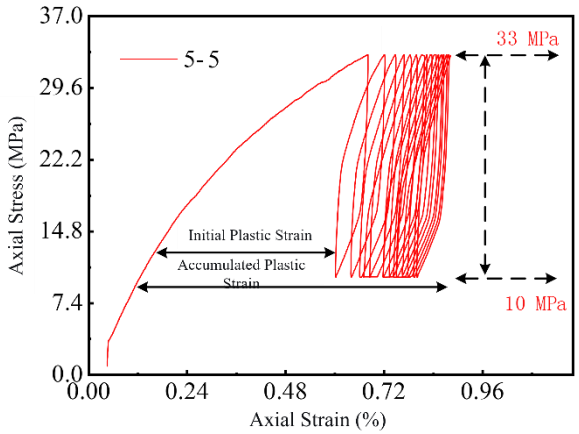

(e) 5-5

Fig. 14 Stress-strain curves of cement in cyclic loading tests

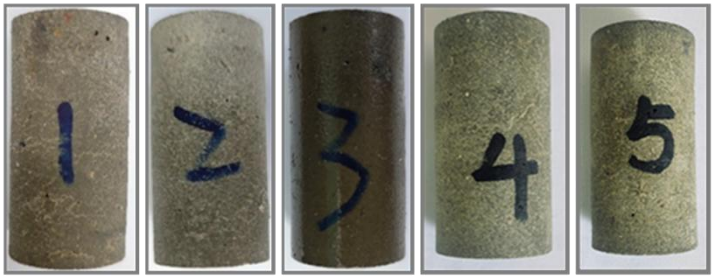

Fig. 15 Morphology of cement specimens after cyclic loading tests

Table 7 Statistical Results of Cyclic Loading Tests

Numble	Compressive Strength(MPa)	Elastic Modulus(GPa)	Poisson's Ratio
5-1	29.84	7.19	0.078
5-2	26.54	3.56	0.035
5-3	29.19	5.06	0.114
5-4	44.17	7.27	0.529
5-5	46.1	7.23	0.129

Fig. 16 presents the results of cumulative plastic strain obtained during the cyclic loading process. The initial plastic strain values after the first cycle for Specimens 5-1, 5-2, 5-3, 5-4, and 5-5 were 0.320%, 0.561%, 0.672%, 0.672%, and 0.683%, respectively. After 15 cycles, these values increased

to 0.393%, 0.714%, 0.731%, 0.734%, and 0.881%, respectively. A linear growth trend in the stress-strain curve of the cement is clearly observed after the first loading-unloading cycle. This is because cement is a heterogeneous and multiphase material inherently containing microcracks, micropores, and other defects. These defects are compacted during the initial cycles, leading to the greatest increase in plastic strain. As cyclic loading and unloading continue, these initial micropores and cracks are further compressed, resulting in a continuous increase in plastic strain.

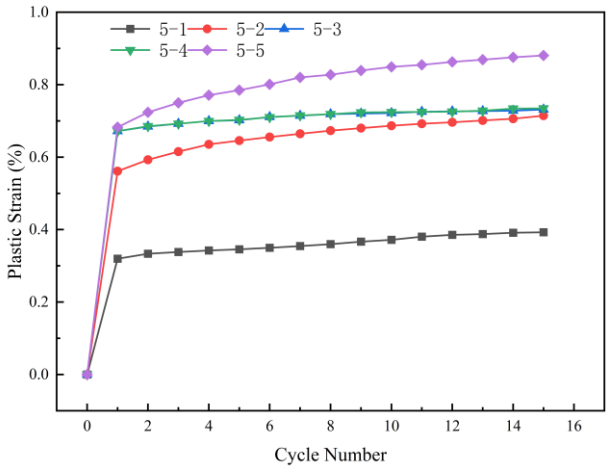

Fig. 16 Cumulative plastic strain during cyclic loading.

Based on the analysis of the results from Fig. 14 and Fig. 16, it can be observed that as the cyclic stress level gradually increases, the hysteresis loop progressively shifts towards larger strain amplitudes during the cyclic loading process. Furthermore, the increase in cyclic stress level also affects, to some extent, the ultimate strength of the cement. This indicates that there is a certain decay pattern in the mechanical stability of the cement sheath under long-term cyclic loading.

A quantitative analysis was conducted on the evolution of plastic strain in cement specimens 5-4 and 5-5 under cyclic loading. The relationship curve between the plastic strain difference and the number of loading cycles was established, as presented in Fig. 17. As the number of cycles increases, the hysteresis loops not only expand but also become denser, indicating that the growth rate of cumulative plastic strain gradually slows down. In the initial stage of cycling, the increment of plastic strain accumulates rapidly and reaches a peak, after which the increment gradually decreases, reflecting the characteristics of nonlinear damage evolution in the material under repeated loading. Taking specimen 5-4 as an example, under a cyclic stress level of 5~28 MPa, the plastic strain increment of the cement reached its maximum value during the first cycle. Subsequently, the plastic strain increment caused by each cycle tended to stabilize, indicating that the upper stress limit is the primary factor affecting the fatigue life of the cement.

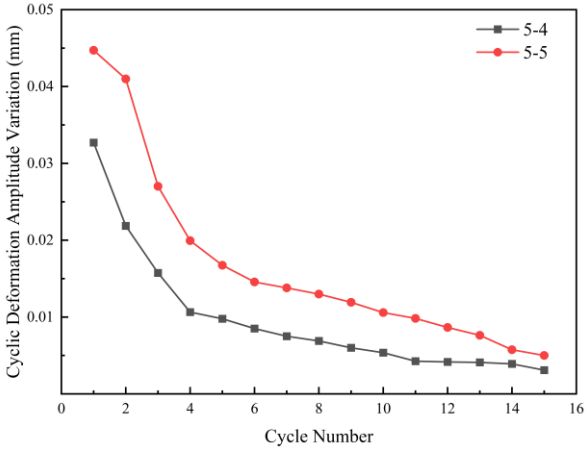

Fig. 17 Plastic strain difference versus number of cycles under cyclic loading-unloading conditions

4. SUMMARY

Upon completion of the tests, both minor radial cracks and shear cracks were observed on the surfaces of the set cement specimens. This confirms that the integrity of the cement sheath has been compromised. In an actual well, such damage can lead to the formation of micro-annuli at the interfaces, providing pathways for gas to migrate from the bottom to the top of the cement sheath, ultimately resulting in annular pressure. The main conclusions obtained under the parameter conditions set in this paper are as follows:

(1) The mechanical properties and failure modes of the set cement are significantly controlled by the stress path and environmental conditions. Under uniaxial compression, the set cement exhibits brittle failure. An increase in the loading rate enhances its compressive strength; however, failure is more abrupt upon reaching the maximum strength. Under triaxial stress conditions, the confining effect significantly improves the compressive strength and overall ductility of the set cement, with the failure mode characterized by multiple shear cracks. Increasing the principal stress loading rate also enhances its strength, whereas increasing the confining pressure strengthens the material but reduces its elastic modulus. A high-temperature environment significantly weakens the mechanical properties of the set cement. At 80°C, the material exhibits a pronounced thermal softening effect, with an earlier yield point and a substantial attenuation of load-bearing capacity. Under cyclic loading simulating injection and production operations, the stress-strain curve of the set cement displays typical hysteresis characteristics. Plastic strain accumulates continuously with an increasing number of cycles, with the accumulation rate being rapid in the initial stage and gradually slowing down thereafter. The upper limit of cyclic stress is the dominant factor affecting its fatigue damage process.

(2) Based on the downhole conditions of gas storage reservoirs, the following engineering guidance can be derived to ensure the structural integrity of the cement sheath. For gas storage wells in high-temperature formations, priority should be given to the selection of high-temperature resistant cement materials to prevent premature material yielding. During the operation of the gas storage facility, controlling the injection-production rate and the upper limit of operating pressure can effectively mitigate the accumulation of plastic strain. Integrating the damage evolution laws revealed in this study provides a basis for predictive maintenance and dynamic adjustment of injection-production parameters, which is conducive to the safe operation of gas storage wells over extended injection-production cycles.

REFERENCES

[1] Wang Y, Feng Y, Zhao Y, et al. Experimental study on cement sheath integrity of UGS wells under cyclic loading[J]. Geoenergy Science and Engineering. 2024, 239212958-.

[2] Zhao Chun, He Mengqi, Chen Xianxue, et al. Experimental study on sealing failure of cement sheath in gas storage wells[J]. China Petroleum Machinery. 2024, 52 (6) : 78-85.

[3] Li Z, Sun J, Luo P, et al. Research on the law of mechanical damage-induced deformation of cement sheaths of a gas storage well[J]. Journal of Natural Gas Science and Engineering. 2017, 4348-57.

[4] LIN Yuanhua, ZHOU Niantao, WANG Xuesong, et al. Experimental study on weakening mechanism of cement sheath interface bonding under alternating loads in gas storage[J]. Deep Earth Energy Science & Technology. 2025, 1(5): 122-130.

[5] SHU Gang, LIU Jian, FENG Feng, et al. Experimental study on failure mechanism of cement sheath in injection production well of gas storage[J]. Drilling Fluid & Completion Fluid. 2020, 37(4): 507-511, 520.

[6] ZHOU Lang, ZENG Qingsong, WANG Chuanlei, et al. An experimental study on the sealing performance of cement sheath in different sections of injection/production wells of an underground gas storage[J]. Natural Gas Industry. 2020, 40(05): 104-108.

[7] Shahvali A, Azin R, Zamani A. Cement design for underground gas storage well completion[J]. Journal of Natural Gas Science and Engineering. 2014, 18149-154.

[8] Yang Y, Yuan B, Sun Q, et al. Mechanical properties of EVA-modified cement for underground gas storage[J]. Journal of Natural Gas Science and Engineering. 2015, 271846-1851.

[9] WANG Xiuling, REN Wenliang, ZHOU Zhanyun, et al. Selection and application of toughening agent used in cementing gas storage well[J]. Drilling Fluid & Completion Fluid. 2017, 34(3): 89-93, 98.

[10] Aluah R, Oni O, Fadairo A, et al. Enhancing the performance of class G cement for subsurface gas storage and well completion: Synergistic impact of North Dakota's fly ash and eggshell powder[J]. Powder Technology. 2024, 440119773-.

[11] Juan L, Donghua S, Shizhong T, et al. Deformation and damage of cement sheath in gas storage wells under cyclic loading[J]. Energy Science & Engineering. 2021, 9(4): 483-501.

[12] WANYAN Qiqi, MAO Tao, WANG Yun, et al. Variation law of cementing stone permeability in gas storage[J]. Fault-Block Oil & Gas Field. 2024, 31(5): 930-935.

[13] FANG Zhongqi, TAN Yuanming, YAN Juntao, et al. Optimization of Cement Slurry System for Gas Storage Based on the Stretching Tensile Strength[J]. Drilling and Production Technology. 2023, 46(3): 128-134.

[14] Liu Jian, Guo Xiaoyang, Li Zaoyuan. Study of the Test Method of Key Mechanical Parameters of Set Cement in the Gas Storage Well[J]. Journal of Southwest Petroleum University: Science & Technology Edition. 2013, 35(6): 115–120.

[15] ZHANG Dan, CHEN Juan, ZHANG Hong, et al. Strength analysis of cement sheath in casing columns of underground gas storage facilities in depleted oil and gas reservoirs[J]. China Petroleum Machinery. 2011, 39(11): 28-32.

[16] Zhang H, Shen R, Yuan G, et al. Cement sheath integrity analysis of underground gas storage well based on elastoplastic theory[J]. Journal of Petroleum Science and Engineering. 2017, 159818-829.

[17] ZHANG Hong, SHEN Ruichen, YUAN Guangjie, et al. Analysis on the elastoplastic of cement sheath in underground gas storage wellbore[J]. 2018, 37(02): 150-156.

[18] Feng B H, Jiang T T, Shang X R, et al. Integrity analysis of the cement sheath in wellbore of underground gas storage based on strain softening model[J]. Safety and Environmental Engineering. 2023, 30(5): 66-75.

[19] Jing J, Tian Y, Zhu X. Integrity of Cement Sheath under Cyclic Injection-Production Loads in Gas Storage Wells[J]. Geotechnical and Geological Engineering. 2024, 43(1): 31-31.

[20] Heng Y, Yuhuan B, Shenglai G, et al. Effects of in-situ stress and elastic parameters of cement sheath in salt rock formation of underground gas storage on seal integrity of cement sheath[J]. Engineering Failure Analysis. 2021,123.

[21] Heng Y, Yuhuan B, ShaoRui J, et al. Effects of creep of the salt rock formation on the failure of cement sheath integrity[J]. Procedia Structural Integrity. 2024, 58144-149.

[22] Tao He, Tongtao Wang, Baodong Shan, et al. Fatigue Damage of Wellbore Cement Sheath in Gas Storage Salt Cavern Under Alternating Internal Pressure[J]. Rock Mechanics and Rock Engineering. 2022, 55: 715-732.

[23] Tao H, Tongtao W, Dongzhou X, et al. Anisotropic damage model of wellbore cement sheath for underground salt cavern gas storage[J]. Construction and Building Materials. 2022, 320.

[24] Su D, Mao T, Huang S, et al. Novel Prediction Method for the Service Life of the Cement Sheath in Gas Storage Wells[J]. SPE Journal. 2025: 1-19.

[25] Yan Y, Lukuan L, Wenyan Y, et al. The Application of Breakthrough Pressure in the Evaluation of the Sealing Ability of Cement–Casing Interface and Cement Matrix in Underground Gas-Storage Wells[J]. Processes. 2022, 10(4): 620-620.